International Journal of Innovative Computing, Information and Control
Volume **21**, Number **5**, October **2025**

ICIC International ©2025 ISSN 1349-4198
pp. **1239–1254**

IDENTIFICATION OF INTERNAL SHORT CIRCUIT FAULTS IN LITHIUM-ION BATTERIES VIA SVMD-RP SPECTRA AND MOBILENETV3

Tinglong Pan[1], Chuanjun Gong[1], Dezhi Xu[2,3,*], Weilin Yang[1] and Yujian Ye[2]

[1]School of Internet of Things Engineering
Jiangnan University
No. 1800, Lihu Avenue, Wuxi 214122, P. R. China
{ tlpan; wlyang }@jiangnan.edu.cn; 6221915008@stu.jiangnan.edu.cn

[2]School of Electrical Engineering
[3]Engineering Research Center of Electrical Transport Technology, Ministry of Education
Southeast University
No. 2, Sipailou, Xuanwu District, Nanjing 210096, P. R. China
yeyujian@seu.edu.cn
*Corresponding author: xudezhi@seu.edu.cn

Received February 2025; revised May 2025

Abstract. *To address the significant risks posed by internal short circuit (ISC) faults in lithium-ion batteries (LIBs) and to ensure the safe operation of LIB systems, this paper proposes an ISC fault identification method based on successive variational mode decomposition (SVMD), recurrence plot (RP) spectra, and the MobileNetV3 network. The method begins by decomposing the voltage signals of LIBs – both under normal conditions and those experiencing ISC faults – using the SVMD algorithm. The resulting intrinsic mode functions (IMFs) are then converted into RP spectra. These spectra are subsequently fed into the MobileNetV3 network for classification. Comparative analysis with other lightweight convolutional neural networks reveals that the proposed approach achieves a significantly higher recognition rate, with an accuracy of 97.2%. Furthermore, the method outperforms competing networks across various performance metrics, demonstrating its effectiveness in identifying ISC faults in LIBs.*

Keywords: Lithium-ion battery, Recurrence plot, Internal short circuit fault, Fault diagnosis, MobileNetV3, Successive variational mode decomposition

1. **Introduction.** Lithium-ion batteries (LIBs) possess several advantages, including high specific energy and power, a wide operating temperature range, and compact volume, making them widely used in transportation and energy storage systems [1]. However, as energy storage devices relying on complex electrochemical reactions, LIBs have been increasingly involved in safety incidents in recent years. This has elevated the enhancement of LIB safety to a critical priority for industry development. Common failures in LIBs include internal short circuit (ISC), external short circuit (ESC), sensor malfunctions, overcharging, over-discharging, and thermal faults. Among these, ISC failures are the most prevalent and indicative, making them a major factor contributing to power battery failures and related accidents [2]. Accurate detection of ISC is, therefore, essential to ensure the secure and reliable operation of battery systems. Diagnostic approaches for ISC failures in LIBs generally fall into three categories: model-driven, knowledge-driven, and

DOI: 10.24507/ijicic.21.05.1239

data-driven methods [3]. Each offers unique strategies to improve safety and operational reliability.

Model-driven fault diagnosis approaches rely heavily on developing accurate models of LIB, as the parameters within these models provide critical insights into potential battery faults. By comparing measured parameters with model-estimated parameters, residual signals are generated, facilitating fault diagnosis through specific evaluation methods [4]. Ouyang et al. [5] proposed a method based on the mean difference model (MDM), utilizing the recursive least squares method to calculate variations in the MDM's open-circuit voltage, resistance, and other characteristic parameters, enabling the detection of internal short circuit (ISC) faults in LIB packs.

Knowledge-driven approaches to fault diagnosis primarily rely on the knowledge and observational data of LIB systems. These methods establish specific relationships between faults and their associated data features using techniques such as fault trees, fuzzy logic, and expert systems, without requiring the development of a detailed system model [6]. Wu et al. [7] utilized changes in electrical parameters and variations in the incremental capacity analysis curve as fault feature vectors. Furthermore, they developed a fault analysis framework based on fuzzy logic to facilitate fault detection in LIBs.

Data-driven approaches to fault diagnosis identify faults by analyzing features extracted from the operational data of LIB [8]. Niu et al. [9] proposed an innovative approach for battery warning and fault diagnosis, utilizing multidimensional, non-dimensional indicators to enhance diagnostic accuracy. Jiang et al. [10] introduced a fault diagnosis method based on the isolation forest algorithm, which demonstrates exceptional capabilities for detecting and warning of thermal runaway in LIB packs. This approach leverages real-world data, including normalized battery voltage, to accurately identify fault types and enable early fault detection, providing robust warnings for both progressive and abrupt faults. Furthermore, Jiang et al. [4] developed a fault assessment procedure that integrates state analysis with early warnings of thermal runaway, offering a comprehensive framework for monitoring and mitigating potential risks in LIB systems. Shang et al. [11] proposed an improved sample Shannon entropy-based method for detecting ISC faults in LIBs. This method identifies early-stage ISC faults by analyzing the modified sample entropy of the battery voltage sequence within a moving window and can predict the fault occurrence time. It demonstrates strong robustness, high reliability, and low computational cost. Qiao et al. [12] developed a data-driven method using machine learning algorithms for diagnosing the early ISC faults based on different relaxation voltage features. The relaxation voltage features of four time scales are extracted and preliminarily selected to train and verify the Gaussian process regression (GPR) model. Furthermore, the particle swarm optimization algorithm is used to optimize the input features for improving the accuracy of the ISC diagnosis. Experimental results show that the diagnostic error of the proposed method is less than 6.5% for early ISC faults.

In conclusion, model-driven fault diagnosis algorithms require high computational precision and face challenges in determining appropriate thresholds. Knowledge-driven fault diagnosis algorithms, on the other hand, often lack sufficient data support, and the external signal features of batteries under different fault conditions exhibit minimal variation [4]. Additionally, the mechanisms behind some battery faults remain poorly understood. Conversely, data-driven fault diagnosis algorithms offer a promising solution for LIB fault detection. These algorithms bypass the need for constructing complex computational models and typically demonstrate high diagnostic efficiency, making them particularly well-suited for LIB fault diagnosis.

Although the conventional data-driven methods have achieved excellent diagnostic performance in LIB fault diagnosis, the computational load required by these methods is too

large to be applied on the battery management system (BMS) side with limited memory. Therefore, this paper proposes a lightweight LIB fault diagnosis method, hoping to solve this problem.

This paper presents a novel approach for detecting ISC faults in LIBs, utilizing successive variational mode decomposition (SVMD), recurrence plot (RP) spectra, and the MobileNetV3 network. The SVMD algorithm and RP transformation are employed to convert voltage data collected from LIBs into RP spectra, which are then processed through the trained MobileNetV3 network to achieve accurate ISC fault identification. Furthermore, this paper compares the proposed method with several classic lightweight convolutional neural networks, evaluating their performance across various metrics. The performance metrics used in this paper include FLOPs, inference time, and recognition rate. FLOPs is used to quantitatively evaluate the computational load of the model. Inference time is used to assess the time spent by the model on detecting a single sample. Recognition rate is used to evaluate the correct identification rate of the model for LIBs with ISC fault and those in normal operation. The comparison highlights the advantages of the proposed approach, particularly in terms of lightweight deployment and recognition accuracy, demonstrating its effectiveness and practicality in LIB fault diagnosis.

2. **Diagnostic Method Description.**

2.1. **VMD.**

VMD is a completely non-recursive, quasi-orthogonal signal analysis method that decomposes a signal into a set of IMFs and solves the variational problem using the variational principle and the alternating direction method of multipliers (ADMM) [8, 13]. The variational problem can be described as follows:

$$\begin{cases} \min\limits_{\{v_k\},\{\omega_k\}} \left\{ \sum\limits_k \left\| \partial_t \left[(\delta(t) + j/\pi t) * v_k(t) \right] e^{-j\omega_k t} \right\|_2^2 \right\} \\ \text{s.t.} \ \sum\limits_k v_k(t) = v(t) \end{cases} \tag{1}$$

As can be seen in Equation (1), $v_k(t)$ represents the IMF component after VMD, $*$ represents the convolution operator, ω_k indicates the centralized frequency of the kth IMF, the signal to be decomposed is denoted by $v(t)$, and $\delta(t)$ represents the unit pulse function.

To solve the above equation, we can introduce a quadratic penalty term τ and Lagrange multipliers β. The following is the augmented Lagrangian expression:

$$\begin{aligned} L\left(v_k, \omega_k, \beta\right) = \tau \sum_k \left\| \partial_t \left[(\delta(t) + j/\pi t) * v_k(t) \right] e^{-j\omega_k t} \right\|_2^2 + \left\| v(t) - \sum_k v_k(t) \right\|_2^2 \\ + \left\langle \beta(t), v(t) - \sum_k v_k(t) \right\rangle \end{aligned} \tag{2}$$

The alternating direction multiplier method can be used to solve the augmented Lagrange equation.

2.2. **SVMD.**

SVMD is a robust and swift approach for adaptive signal decomposition. In a seamless process, all the IMFs of the signal are extracted by SVMD. Compared to VMD, pre-existing of the volume of modes is not required by SVMD, and it exhibits reduced computational complexity. The decomposition process of the signal is more automated and efficient with SVMD. SVMD is an algorithm for continuously discovering modes. This continuous mode discovery method helps improve convergence speed. The signal decomposition here is achieved by continuously applying variational mode extraction (VME)

to signal, with additional constraints added to prevent convergence to already extracted modes [14, 15]. The procedure proceeds until all modes have been isolated. Alternatively, it terminates when the reconstruction error – evaluating the discrepancy between the input signal and the aggregate sum of the modes – drops below an established threshold. Enhancing the accuracy of the decomposition is this iterative refinement.

The process of SVMD can be described as follows.

Assume voltage signal of LIBs $v(t)$ can be divided into two components, the mth decomposed mode $v_m(t)$ and the residual signal $v_n(t)$.

$$v(t) = v_m(t) + v_n(t) \tag{3}$$

As can be seen in Equation (3), the residual signal $v_n(t)$ in the equation is the $v(t)$ excluding $v_m(t)$, and it made up of two parts: the obtained modes and the untreated portion of the input signal $v_u(t)$.

$$v_n(t) = \sum_{i=1:m-1} v_i(t) + v_u(t) \tag{4}$$

As dictated by principle of VME, the decomposed modes should be centered around a central frequency. Therefore, the modes extracted in the mth iteration satisfy the following minimization criterion:

$$D_1 = \left\| \partial_t \left[\left(\delta(t) + \frac{j}{\pi t} \right) * v_m(t) \right] e^{-j\omega_m t} \right\|_2^2 \tag{5}$$

In Equation (5), ω_m is the center frequency of the mth mode decomposition, and $*$ represents the convolution operator.

At the effective component frequency of the mth mode decomposition $v_m(t)$, the energy of $v_n(t)$ should be minimized. This constraint will work by utilizing a filter with an appropriate frequency response of $\hat{\gamma}_m(\omega)$. The frequency response of $\hat{\gamma}_m(\omega)$ filter can be designed as:

$$\hat{\gamma}_m(\omega) = \frac{1}{\tau \left(\omega - \omega_m\right)^2} \tag{6}$$

Therefore, the second minimization criterion D_2 is

$$D_2 = \|\gamma_m(t) * v_n(t)\|_2^2 \tag{7}$$

In Equation (7), $\gamma_m(t)$ is the impulse response of the designed filter.

By minimizing the two criteria D_1 and D_2, the mth decomposed mode can be obtained. However, this mode might be one of the $m-1$ modes previously obtained. In order to avoid such situations, $v_m(t)$ should have less energy near the center frequencies of the previously obtained modes. This constraint is similar to the constraint of D_2, and the frequency response of the filter used is

$$\hat{\gamma}_i(\omega) = \frac{1}{\tau \left(\omega - \omega_i\right)^2}; \quad i = 1, 2, \ldots, m-1 \tag{8}$$

The established constraint is

$$D_3 = \sum_{i=1}^{m-1} \|\gamma_i(t) * v_m(t)\|_2^2 \tag{9}$$

In Equation (9), $\gamma_i(t)$ is the impulse response of the designed filter. To ensure that the decomposed m modes and the unprocessed part of the signal can be reconstructed into the original signal, the final constraint is applied, namely

$$v(t) = v_m(t) + v_u(t) + \sum_{i=1:m-1} v_i(t) \tag{10}$$

When the constraints of the $m-1$ decomposed modes are known, the mth mode is identified. This mode can then be converted into a constrained minimization problem. According to the constraints above, the combination of D_1, D_2 and D_3 is minimized:

$$\begin{aligned} &\min_{v_m,\omega_m,v_n} \{\tau D_1 + D_2 + D_3\} \\ &\text{subject to } v_m(t) + v_n(t) = v(t) \end{aligned} \tag{11}$$

In Equation (11), τ is a parameter for balancing D_1, D_2 and D_3. It can be determined utilizing the Lagrangian multiplier approach. To formulate the augmented Lagrangian function, the quadratic penalty term is integrated with Lagrange multipliers. This approach accelerates convergence and boosts reconstruction performance amid noise.

$$\begin{aligned} L\left(v_m, \omega_m, \tau\right) = \tau D_1 + D_2 + D_3 + \left\| v(t) - \left(v_m(t) + v_u(t) + \sum_{i=1}^{m-1} v_i(t) \right) \right\|_2^2 \\ + \left\langle \tau(t), v(t) - \left(v_m(t) + v_u(t) + \sum_{i=1}^{m-1} v_i(t) \right) \right\rangle \end{aligned} \tag{12}$$

In Equation (12), τ is Lagrange multiplier. Similar to VME, the minimization problem can be solved utilizing ADMM. The result of $v_m(\omega)$ after $n+1$ iterations can be described below:

$$\hat{v}_m^{n+1}(\omega) = \frac{\hat{v}(\omega) + \tau^2 \left(\omega - \omega_m^n\right)^4 \hat{v}_m^n(\omega) + \frac{\hat{\beta}(\omega)}{2}}{\left[1 + \tau^2 \left(\omega - \omega_m^n\right)^4\right] \left[1 + 2\tau \left(\omega - \omega_m^n\right)^2 + \sum_{i=1}^{m-1} \frac{1}{\tau^2 (\omega - \omega_i)^4}\right]} \tag{13}$$

where the equation for ω_m can be approximated as

$$\omega_m^{n+1} = \frac{\int_0^\infty \omega \left|\hat{v}_m^{n+1}(\omega)\right|^2 d\omega}{\int_0^\infty \left|\hat{v}_m^{n+1}(\omega)\right|^2 d\omega} \tag{14}$$

Similar to VME, the equations for updating the Lagrange multipliers β are obtained based on dual ascent:

$$\hat{\beta}^{n+1} = \hat{\beta}^n + \tau \left[\hat{v}(\omega) - \left(\hat{v}_m^{n+1}(\omega) + v_u^{n+1}(t) + \sum_{i=1}^{m-1} v_i^{n+1}(\omega) \right) \right] \tag{15}$$

In the process of minimizing the function $\hat{v}_u(t)$ using the Parseval inequality, the following equation can be described below:

$$\begin{aligned} \hat{v}_u^{n+1}(\omega) = &\frac{\tau^2 \left(\omega - \omega_m^{n+1}\right)^4 \left(\hat{v}(\omega) - \hat{v}_m^{n+1}(\omega)\right)}{1 + \tau^2 \left(\omega - \omega_m^n\right)^4} \\ &- \frac{\tau^2 \left(\omega - \omega_m^{n+1}\right)^4 \left(\sum_{i=1}^{m-1} \hat{v}_i^{n+1}(\omega) - \frac{\hat{\beta}(\omega)}{2}\right) + \sum_{i=1}^{m-1} \hat{v}_i(\omega)}{1 + \tau^2 \left(\omega - \omega_m^n\right)^4} \end{aligned} \tag{16}$$

By substituting Equation (16) for $v_u(t)$, the following equation can be obtained:

$$\begin{cases} G(\omega) = \dfrac{\left(\hat{v}(\omega) - \hat{v}_m^{n+1}(\omega) - \sum_{i=1}^{m-1} \hat{v}_i(\omega) + \frac{\hat{\beta}(\omega)}{2}\right)}{1 + \frac{1}{\tau^2 (\omega - \omega_m^n)^4}} - \dfrac{\sum_{i=1}^{m-1} \hat{v}_i(\omega)}{1 + \tau^2 \left(\omega - \omega_L^{n+1}\right)^4} \\ \hat{\beta}^{n+1} = \hat{\beta}^n + \tau \left[\hat{v}(\omega) - \hat{v}_m^{n+1}(\omega) - G(\omega) - \sum_{i=1}^{m-1} v_i^{n+1}(\omega) \right] \end{cases} \tag{17}$$

The complete iterative process is as follows.

1) Input the voltage signal of LIBs $v(t)$, set τ, ε_1, ε_2 and σ^2, and initialize the number of modes m to 0.
2) Set $m = m + 1$, initialize $\hat{v}_m^1$, $\hat{\beta}^1$, ω_m^1, set n equal to 0, μ outer loop begins.
3) Set $n = n + 1$, update $\hat{v}_m$ for all $\omega \geq 0$ according to Equation (13), update ω_m according to Equation (14), update $\hat{\beta}^{n+1}$ according to Equation (17), and start the inner loop.
4) The inner loop ends when the iteration converges to $\frac{\left\|\hat{v}_m^{n+1}-\hat{v}_m^n\right\|_2^2}{\|\hat{v}_m^n\|_2^2} < \varepsilon_1$, ε_1 represents the convergence threshold of the inner loop, and this paper sets to 1e-4.
5) The outer loop ends when the iteration converges to $\frac{\left|\sigma^2-\frac{1}{T}\left\|\left(v(t)-\sum_{l=1:} v_l(t)\right)\right\|_2^2\right|}{\sigma^2} < \varepsilon_2$, ε_2 represents the convergence threshold of the outer loop, and this paper sets to 1e-3.

2.3. **Transformation of RP.** After decomposing the voltage signal using SVMD, the following can be obtained:

$$f(t) = \sum_{i=1}^{k} u_i(t) \tag{18}$$

After decomposing the IMF components obtained from SVMD decomposition, RP transformation is applied. Formally proposed by Eckmann et al. [16], RP is a nonlinear signal analysis method extensively employed to reveal the periodic patterns of trajectories in the state space [17]. It is a commonly used processing and analysis method in the field of non-stationary signal analysis [18]. RP can effectively reflect the similarity and stability of the internal structure within signal time series. Recursion exists in the original space. After the phase space is reconstructed, the points in the phase space can be intuitively displayed in the form of two-dimensional graphics, and the resulting two-dimensional graphics is RP.

The algorithmic steps for generating an RP are as follows.

Assuming vector $U = (u_1, u_2, \ldots, u_n)$ represents a time series signal of length N.

1) By performing theoretical calculations on the collected time series, suitable embedding dimension m and delay time τ can be determined, thereby reconstructing the phase space. The reconstructed space is given by

$$X_i = [u_i, u_{i+\tau}, \ldots, u_{i+(m-1)\tau}] \tag{19}$$

In Equation (19), $i = 1, 2, \ldots, n - (m-1)\tau$.

2) Calculate the distance (vector norm) between any two states x_i and x_j in the reconstructed phase space:

$$S_{ij} = \|x_i - x_j\| \tag{20}$$

In Equation (20), $j = 1, 2, \ldots, n - (m-1)\tau$, and $\| \|$ is table norm.

3) Calculate the recurrence value

$$R(i,j) = \Theta(\varepsilon - S_{ij}) \tag{21}$$

In Equation (21), the threshold ε represents a preset distance, making $R(i,j) \in (0,1)$, and Θ indicates Heaviside function.

$$\Theta(u) = \begin{cases} 0, & u \leq 0 \\ 1, & u > 0 \end{cases} \tag{22}$$

Using the above steps, recurrence plots can be obtained. When $R(i,j) = 1$, a black dot appears on RP. Conversely, when $R(i,j) = 0$, a white dot is shown [19]. Black and white dots are the most basic representations of a recurrence plot. By depicting the plot with black and white dots, the characteristics of the time series can be reflected.

2.4. **MobileNetV3 network.** Introduced by the Google team in 2019, a highly efficient and lightweight network for mobile and embedded applications is MobileNetV3. Its characteristics include having fewer parameters, reduced computational requirements, and shorter inference time, making it highly suitable for scenarios with limited storage space and power constraints. Compared to MobileNetV1 and V2, MobileNetV3 introduced three main updates.

1) Optimizing Network Architecture: Introducing Platform-Aware NAS and NetAdapt [20].

2) Improving Nonlinear Activation Functions: Introducing a new nonlinear activation function h-swish. In the first half of the MobileNetV3 network, swish is used, while h-swish is applied in the latter half.

3) Redesigned Expensive Layers: Redesigned and modified the interactions at the end of the network, adjusting the structural sequence of the network [21, 22].

Figure 1 shows the network structure of MobileNetV3. As input to MobileNetV3, images are used, the input undergoes convolutional operations, followed by batch normalization (BN) layers and the h-swish, before entering the bottleneck (Bneck) structure of the network. MobileNetV3 is divided into two versions: large and small. The differences between the two versions lie in the number of Bnecks and their internal parameters. This article considers the lightweight deployment of fault diagnosis algorithms and selects the MobileNetV3-small version. After average pooling, the output is then passed through a BN layer in the fully connected (FC) layer and activated using h-swish to generate the feature vector [23].

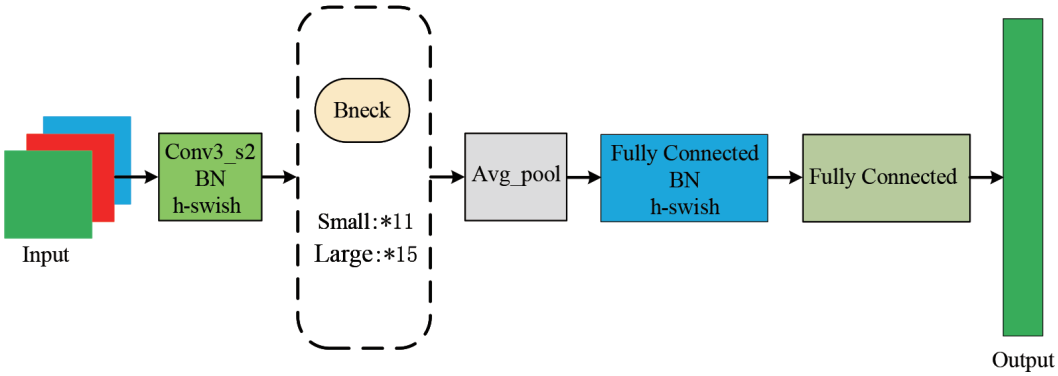

FIGURE 1. MobileNetV3 network structure

Building on the MobileNetV2 framework, MobileNetV3 introduces lightweight attention modules. These modules, based on squeeze and excitation, are integrated into the Bneck structure to enhance efficiency. These modules are placed after the depthwise (DW) filters in the expansion phase. As shown in Figure 2, MobileNetV3 employs platform-aware NAS to optimize the global network structure by refining each individual network block. The number of filters is then searched using the NetAdapt algorithm, which is a complement to platform-aware NAS and authorizes the individual layers of the network to be adapted in a sequential manner.

MobileNetV3 also makes specific optimizations such as reducing the number of convolutional filters from 32 to 16 in the first convolutional layer and streamlining the Last Stage. Furthermore, after redesigning the expensive layer structure, MobileNetV3 greatly reduces the model's inference time.

MobileNet series' core idea lies in the utilization of DW separable convolutions, which is also the primary reason for its lightweight characteristics. As shown in Figure 3, DW

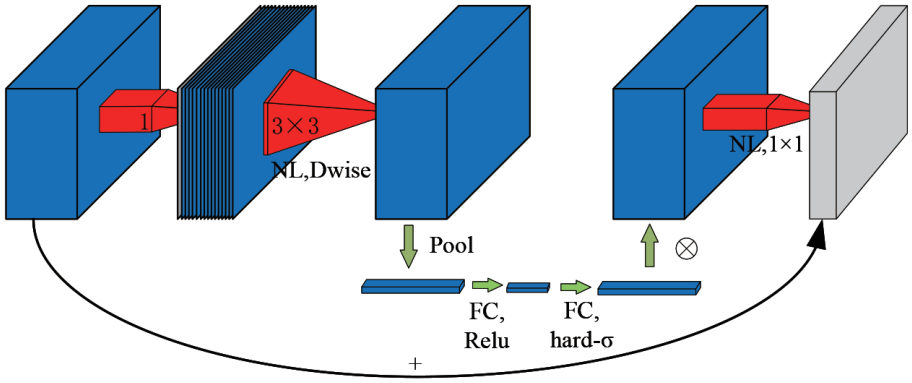

FIGURE 2. The schematic diagram of the lightweight attention module

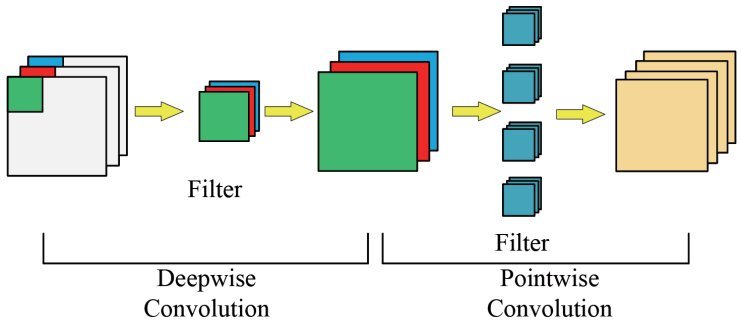

FIGURE 3. Deep separable convolution

separable convolution decomposes a standard convolution into two separate processes: DW convolution and pointwise (PW) convolution.

In standard convolution, a three-dimensional convolution kernel is employed to extract feature information simultaneously from both the spatial dimensions and channel dimensions. However, in DW separable convolution, it consists of DW convolution and PW convolution. The DW convolution is responsible for extracting feature information along the spatial dimensions, and the PW convolution, building upon output of the DW convolution, computes a linear combination of the outputs, further extracting feature information along the channel dimension [21, 24]. By simplifying calculations and decreasing the parameter count, this decomposition streamlines the model, making it more lightweight while preserving its representational capacity.

2.5. **Fault diagnosis process.** The fault diagnosis algorithm derived from SVMD-RP spectra and MobileNetV3 network introduced in this paper is shown in Table 1.

3. **Data Description.** The voltage data analyzed in this study originates from the Open Laboratory of the National Big Data Alliance of New Energy Vehicles (NDANEV) platform. This platform is responsible for monitoring new energy vehicles (EVs) across the country. It provides insights into both broad metrics, such as the total number of vehicles connected to the national network and those currently online, as well as specific operational details for individual vehicles, including battery status, temperature, and other relevant parameters [25, 26, 27]. The platform's architecture is illustrated in Figure 4.

The platform collects actual operational data from EVs equipped with onboard terminals that gather and process various data types. This information is transmitted to the NDANEV system through the GB/T 32960 protocol, and is stored and analyzed in the system. The collected data comprises both dynamic and static categories. Dynamic data

TABLE 1. Fault diagnosis algorithm

Algorithm: Fault diagnosis algorithm
Input: Voltage signals of LIBs
Output: The performance metrics of fault diagnosis algorithms
1. Obtaining SVMD-RP spectra using SVMD and RP transformation.
2. Randomly splitting the SVMD-RP spectra into training dataset V_{train} and validation dataset V_{val}.
3. Constructing the MobileNetV3 network and train it using V_{train}.
4. Initializing the training parameters. The cross entropy loss function and the Adam optimizer with a learning rate of 0.001, the number of training epochs is set to 50.
5. Adjusting model parameters through backpropagation to minimize loss function progressively.
6. Employing the optimized MobileNetV3 network to identify validation dataset V_{val} and obtain the performance metrics.

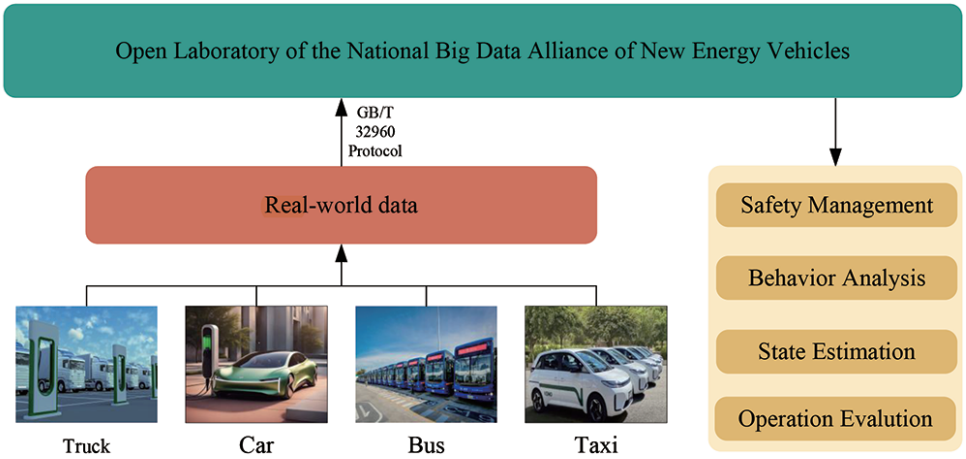

FIGURE 4. The schematic of the NDANEV platform

primarily includes parameters of the battery system, such as voltage, current, temperature, and state of charge (SOC). In contrast, static data encompasses details like the VIN, vehicle model, and other related information. However, due to limitations in vehicle sensor placement and capabilities, not all characteristics of the battery systems can be captured [4, 28]. The careful selection of features is critical for effectively assessing the state of LIBs. Such selection plays a significant role in ensuring accurate analysis and evaluation of battery performance and health.

As shown in Table 2, instantaneous current is highly influenced by driving behavior, and for a series-connected battery pack, the current across all individual cells remains consistent. However, detecting ISC faults in LIB based on current alone is challenging. The SOC represents the overall condition of LIB packs, but subtle variations in individual cells are not easily discernible through SOC measurements. Additionally, because vehicle temperature sensors do not sample data at the level of individual cells, there is a delay in capturing internal temperature changes on the battery's surface. Consequently, temperature measurements only provide partial insight into the thermal characteristics of LIBs. In contrast, the voltage of each individual cell serves as the most direct indicator of a cell's condition, making it an ideal parameter for diagnosing battery faults. This study,

TABLE 2. Characteristic state vector selection

Type of data	Features
Current	Current depends on driving behavior
Cell Voltage	Sensitive to state changes
SOC	Battery packs status
Temperature	Measures the temperature at a fixed location

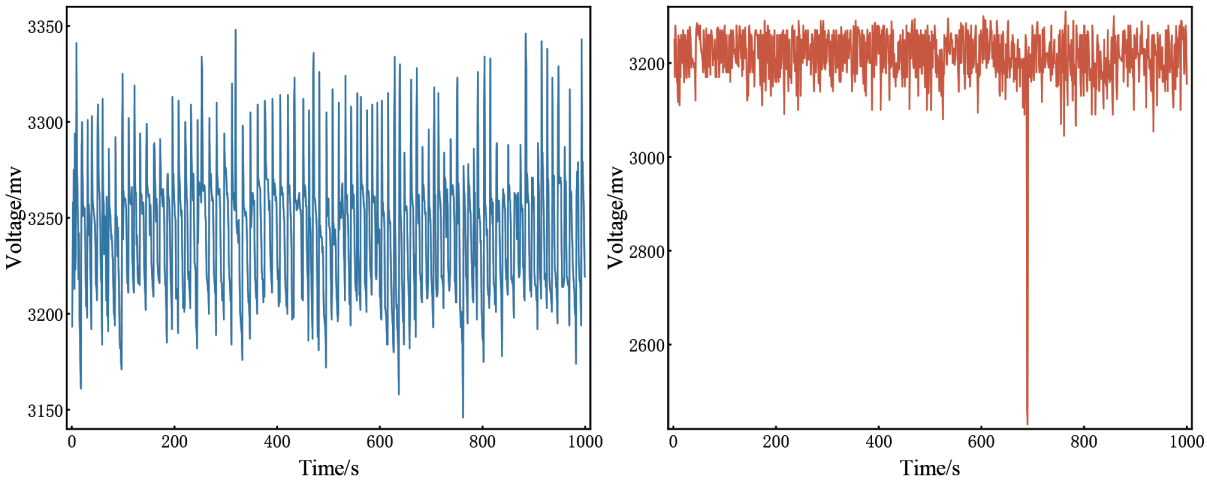

(a) (b)

FIGURE 5. Voltage signals of LIBs: (a) Normal voltage signal of LIB; (b) voltage signal of LIB with ISC fault

therefore, selects individual cell voltage as the primary feature parameter for ISC fault diagnosis.

To minimize the impact of various battery types and external factors on the results, a dataset was curated from electric vehicles (EVs) using the same type of battery. This ensures consistency across models, reducing variability. The dataset includes EVs manufactured by a specific automotive company and monitored through the NDANEV platform. The selected battery type is a ternary lithium battery with a nominal voltage of 3.2 V. The dataset comprises 1000 voltage signal samples collected under normal conditions and during ISC faults. Figure 5 illustrates these voltage signals.

For this study, 60 sets of data were selected for each condition, resulting in a total of 120 datasets. Of these, 30 sets for each condition were randomly chosen for training the network. The remaining 60 sets were reserved as the testing set to validate the proposed approach.

4. **Generation of SVMD-RP Spectra and Performance Metrics of Different Network.** The voltage signals of LIBs are adaptively decomposed using SVMD algorithm, with parameters β set to 20000 and a convergence error threshold of 1e-6. The SVMD decomposition results are introduced in Figure 6.

As illustrated in Figure 6, the voltage signals of LIBs are adaptively decomposed into three distinct components using SVMD algorithm: Mode 1, Mode 2, and Mode 3, which are extracted sequentially from low to high frequencies. Mode 1, the static component, represents the long-term trend or the fundamental component of the voltage signal from LIBs. Mode 2 and Mode 3 both represent dynamic components, characterizing the rapid variations and short-term fluctuations in the voltage signals of LIBs.

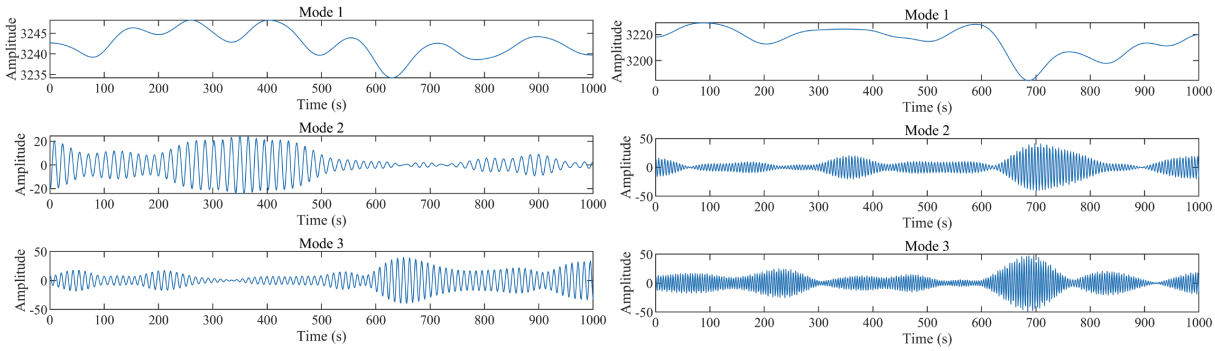

(a) (b)

FIGURE 6. Voltage signals of LIB by SVMD: (a) Normal voltage signal of LIB by SVMD; (b) voltage signal of LIB with ISC fault by SVMD

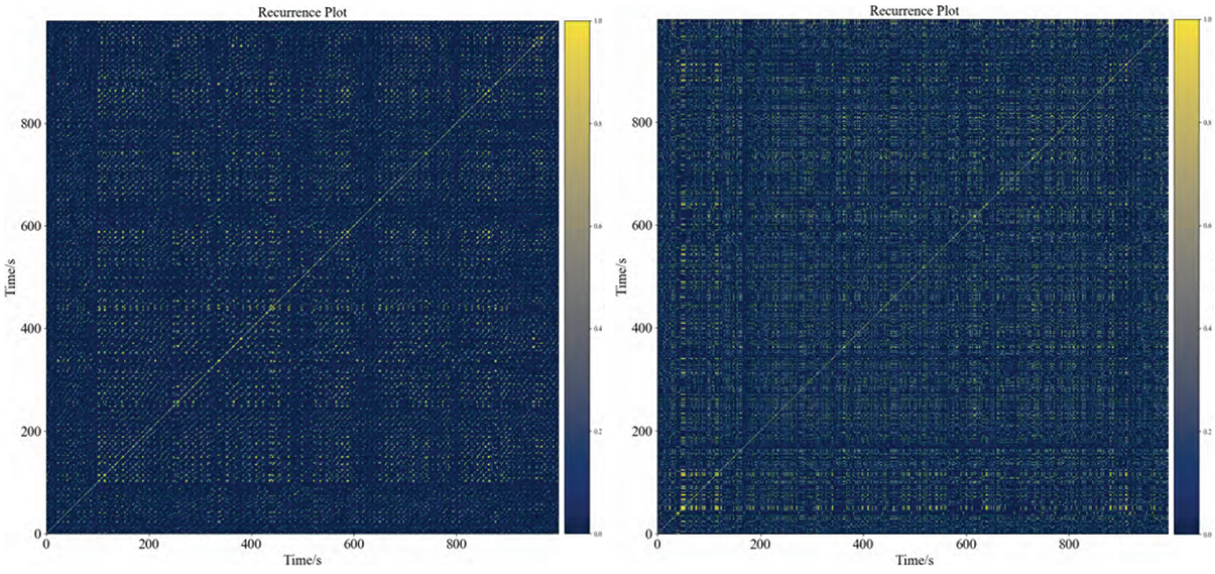

(a) (b)

FIGURE 7. RP spectra: (a) RP of LIB voltage signal under normal condition; (b) RP of LIB voltage signal with ISC fault

Under normal conditions, the trend of the static component Mode 1 is not obvious, but under the circumstances of an ISC fault in LIBs, this trend component will show a clear downward trend before the fault occurs. Relatively, under normal conditions, the dynamic component Mode 2, Mode 3 do not change significantly, but in the presence of ISC faults in the voltage signals of LIBs, the dynamic component will show significant fluctuations before the fault occurs.

After decomposing the voltage signals of the LIBs using SVMD, the IMFs of the voltage signal are obtained. The IMFs of each voltage signal are then transformed into RPs, resulting in the RP spectra shown in Figure 7. After obtaining the RP spectra, it is transformed into a 256×256 matrix as MobileNetV3's input. The MobileNetV3 network is then utilized to automatically extract the intrinsic features of the pixel data in the plot. Finally, these features are mapped to sample labels, enabling the identification of normal LIBs and those with ISC faults.

In this paper, validation dataset V_{val} is selected to verify the introduced approach. The validation dataset consists of 60 sets of data, including 30 sets of voltage signals under

normal conditions and 30 sets of voltage signals when ISC fault occurs in LIBs. To verify the advantages of the introduced approach, other classical lightweight convolutional neural network models are selected and compared.

To further validate the effectiveness of the approach described, this paper undertakes a comparative analysis of other three established lightweight convolutional neural network, ShuffleNetV2, LeNet, and EfficientNetV2 – using them to train and recognize lithium-ion battery voltage signals under both normal and internal short-circuit fault conditions. The training is conducted using a standardized dataset, with all models employing stochastic gradient descent for optimization and maintaining identical training parameters as those used for MobileNetV3 in this study.

The performance metrics for the four models are detailed in the accompanying Table 3. Analysis reveals that, despite LeNet's relatively low floating-point operation volume of 7.69 MB, its fault recognition accuracy is limited to 87.6%, which is inadequate for effective fault diagnosis. Conversely, MobileNetV3 demonstrates a superior fault recognition rate of 97.2%, marginally outperforming EfficientNetV2 and ShuffleNetV2. Moreover, MobileNetV3's FLOPs is lower than that of the latter two models, and it achieves a notably efficient inference time of 3.04 ms. This performance underscores MobileNetV3's exceptional suitability for rapid, lightweight deployment in fault detection applications.

TABLE 3. The performance metrics of different network

Network	FLOPs	Inference time	Recognition rate
ShuffleNetV2	26.78 MB	8.28 ms	92.1%
LeNet	7.69 MB	10.54 ms	87.6%
EfficientNetV2	18.95 MB	16.04 ms	95.4%
MobileNetV3	12.24 MB	3.04 ms	97.2%

As the number of iterations increases, the training loss value of the MobileNetV3 network gradually decreases and quickly stabilizes, as shown in Figure 8. The training accuracy curve stabilizes after reaching 30 iterations. At this point, further increasing the number of iterations would consume significant computational time. Therefore, taking redundancy into consideration, this paper sets the number of iterations to 50.

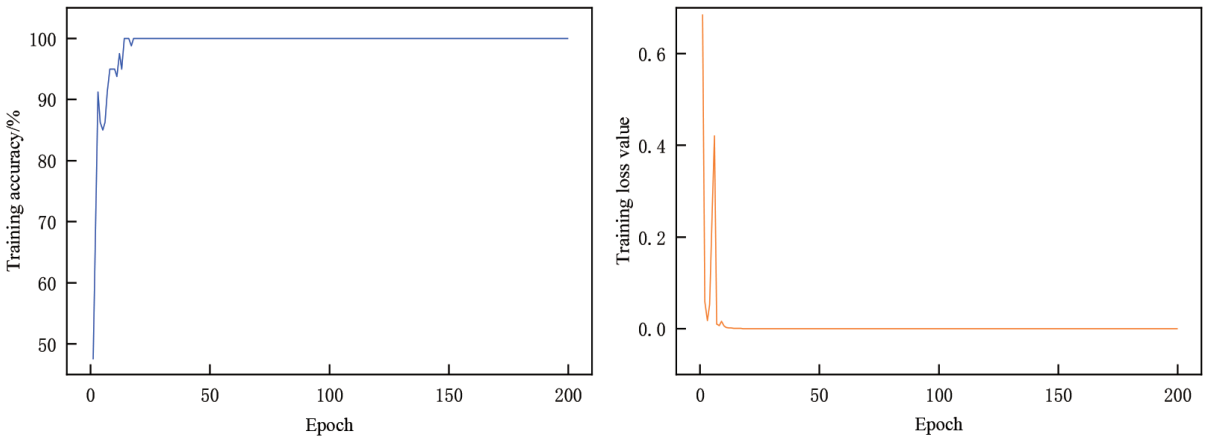

(a) (b)

FIGURE 8. MobileNetV3 training process: (a) Training accuracy; (b) training loss value

5. **Conclusion.** This paper utilizes voltage signals of LIB in both normal states and those experiencing ISC faults, collected from real vehicles via the NDANEV platform, as input for the diagnostic algorithm. The voltage signals are decomposed using SVMD to extract IMF. These IMFs are then transformed into RP spectra. The lightweight MobileNetV3 model is employed to extract features from the RP spectra, enabling the identification of LIB voltage signals corresponding to normal states and ISC faults. Additionally, the proposed method is compared with other classical lightweight CNN models. Although the proposed method demonstrates promising performance in terms of inference time, recognition rate, and FLOPs for LIBs with ISC fault detection, several challenges remain. Specifically, while this study focuses on ISC fault identification, LIBs can experience various complex fault types, making accurate fault classification a challenging task. Addressing these complexities remains a crucial research challenge, and future work will prioritize the development of more comprehensive fault diagnosis solutions to enhance the reliability and robustness of BMS.

The notable characteristics and contributions of this work are summarized as follows.

1) Time Imaging Technology for ISC Fault Detection. This study demonstrates the effective use of time imaging technology for detecting and identifying ISC faults in LIBs. By converting one-dimensional time-series data into two-dimensional RP spectra, the method provides richer information, significantly enhancing the accuracy of ISC fault classification in LIBs.
2) Development of Hybrid Models. By integrating classical lightweight CNN models, hybrid frameworks such as SVMD-RP-LeNet are proposed. These hybrid models combine the strengths of SVMD, RP transformation, and lightweight CNNs, offering robust fault detection performance.
3) Expanding Research on ISC Fault Identification. This work broadens the methodological landscape for ISC fault identification in LIBs, contributing to safer LIB operation and encouraging further advancements in diagnostic technology.

Acknowledgment. This paper was supported in part by the National Natural Science Foundation of China under Grant 62222307, in part by the National Natural Science Foundation of China under Grant 61973140, in part by the Natural Science Foundation of Jiangsu Province under Grant BK20211235.

REFERENCES

[1] T. Lin, Z. Chen, C. Zheng, D. Huang and S. Zhou, Fault diagnosis of lithium-ion battery pack based on hybrid system and dual extended Kalman filter algorithm, *IEEE Transactions on Transportation Electrification*, vol.7, no.1, pp.26-36, 2020.

[2] J. Zhao, X. Feng, M.-K. Tran, M. Fowler, M. Ouyang and A. F. Burke, Battery safety: Fault diagnosis from laboratory to real world, *Journal of Power Sources*, vol.598, 234111, 2024.

[3] R. Xiong, W. Sun, Q. Yu and F. Sun, Research progress, challenges and prospects of fault diagnosis on battery system of electric vehicles, *Applied Energy*, vol.279, 115855, 2020.

[4] L. Jiang, Z. Deng, X. Tang, L. Hu, X. Lin and X. Hu, Data-driven fault diagnosis and thermal runaway warning for battery packs using real-world vehicle data, *Energy*, vol.234, 121266, 2021.

[5] M. Ouyang, M. Zhang, X. Feng, L. Lu, J. Li, X. He and Y. Zheng, Internal short circuit detection for battery pack using equivalent parameter and consistency method, *Journal of Power Sources*, vol.294, pp.272-283, 2015.

[6] M. Held and R. Brönnimann, Safe cell, safe battery? Battery fire investigation using FMEA, FTA and practical experiments, *Microelectronics Reliability*, vol.64, pp.705-710, 2016.

[7] C. Wu, C. Zhu and Y. Ge, A new fault diagnosis and prognosis technology for high-power lithium-ion battery, *IEEE Transactions on Plasma Science*, vol.45, no.7, pp.1533-1538, 2017.

[8] W. Wei, X. Zhang and L. Yang, Full-cycle state evaluation of S700K switch machine based on residual network and fuzzy clustering, *International Journal of Innovative Computing, Information and Control*, vol.18, no.4, pp.1203-1216, 2022.
[9] L. Niu, J. Du, S. Li, J. Wang, C. Zhang and Y. Jiang, An online fault diagnosis method for lithium-ion batteries based on signal decomposition and dimensionless indicators selection, *Journal of Energy Storage*, vol.83, 110590, 2024.
[10] J. Jiang, T. Li, C. Chang, C. Yang and L. Liao, Fault diagnosis method for lithium-ion batteries in electric vehicles based on isolated forest algorithm, *Journal of Energy Storage*, vol.50, 104177, 2022.
[11] Y. Shang, G. Lu, Y. Kang, Z. Zhou, B. Duan and C. Zhang, A multi-fault diagnosis method based on modified sample entropy for lithium-ion battery strings, *Journal of Power Sources*, vol.446, 227275, 2020.
[12] D. Qiao, X. Wei, B. Jiang, W. Fan, X. Lai, Y. Zheng and H. Dai, Quantitative diagnosis of internal short circuit for lithium-ion batteries using relaxation voltage, *IEEE Transactions on Industrial Electronics*, vol.71, no.10, pp.13201-13210, 2024.
[13] K. Dragomiretskiy and D. Zosso, Variational mode decomposition, *IEEE Transactions on Signal Processing*, vol.62, no.3, pp.531-544, 2013.
[14] M. Nazari and S. M. Sakhaei, Successive variational mode decomposition, *Signal Processing*, vol.174, 107610, 2020.
[15] S. Parri and K. Teeparthi, SVMD-TF-QS: An efficient and novel hybrid methodology for the wind speed prediction, *Expert Systems with Applications*, 123516, 2024.
[16] J.-P. Eckmann, S. O. Kamphorst and D. Ruelle, Recurrence plots of dynamical systems, *Europhysics Letters*, vol.4, no.9, 973, 1987.
[17] B. M. Mathunjwa, Y.-T. Lin, C.-H. Lin, M. F. Abbod and J.-S. Shieh, ECG arrhythmia classification by using a recurrence plot and convolutional neural network, *Biomedical Signal Processing and Control*, vol.64, 102262, 2021.
[18] R. Bai, Z. Meng, Q. Xu and F. Fan, Fractional fourier and time domain recurrence plot fusion combining convolutional neural network for bearing fault diagnosis under variable working conditions, *Reliability Engineering & System Safety*, vol.232, 109076, 2023.
[19] Z.-J. Peng, C. Zhang and Y.-X. Tian, Crude oil price time series forecasting: A novel approach based on variational mode decomposition, time-series imaging, and deep learning, *IEEE Access*, 2023.
[20] T.-J. Yang, A. Howard, B. Chen, X. Zhang, A. Go, M. Sandler, V. Sze and H. Adam, NetAdapt: Platform-aware neural network adaptation for mobile applications, *Proc. of the European Conference on Computer Vision (ECCV)*, pp.285-300, 2018.
[21] A. Howard, M. Sandler, G. Chu, L.-C. Chen, B. Chen, M. Tan, W. Wang, Y. Zhu, R. Pang, V. Vasudevan et al., Searching for MobileNetV3, *Proc. of the IEEE/CVF International Conference on Computer Vision*, pp.1314-1324, 2019.
[22] Y. Zhang, C. Xu, R. Du, Q. Kong, D. Li and C. Liu, MSIF-MobileNetV3: An improved MobileNetV3 based on multi-scale information fusion for fish feeding behavior analysis, *Aquacultural Engineering*, vol.102, 102338, 2023.
[23] X. Luo, D. Xia, R. Tao and Y. Shi, Fabric image retrieval based on fine-grained features, *Journal of Donghua University (English Edition)*, vol.41, no.2, 2024.
[24] S. Qian, C. Ning and Y. Hu, MobileNetV3 for image classification, *2021 IEEE 2nd International Conference on Big Data, Artificial Intelligence and Internet of Things Engineering (ICBAIE)*, pp.490-497, 2021.
[25] Z. Sun, Z. Wang, Y. Chen, P. Liu, S. Wang, Z. Zhang and D. G. Dorrell, Modified relative entropy-based lithium-ion battery pack online short-circuit detection for electric vehicle, *IEEE Transactions on Transportation Electrification*, vol.8, no.2, pp.1710-1723, 2021.
[26] L. Zhou, Y. Zhao, D. Li and Z. Wang, State-of-health estimation for $LiFePo_4$ battery system on real-world electric vehicles considering aging stage, *IEEE Transactions on Transportation Electrification*, vol.8, no.2, pp.1724-1733, 2021.
[27] Q. Wang, Z. Wang, L. Zhang, P. Liu and Z. Zhang, A novel consistency evaluation method for series-connected battery systems based on real-world operation data, *IEEE Transactions on Transportation Electrification*, vol.7, no.2, pp.437-451, 2020.
[28] Z. Jia, Z. Wang, Z. Sun, P. Liu, X. Zhu and F. Sun, A data-driven approach for battery system safety risk evaluation based on real-world electric vehicle operating data, *IEEE Transactions on Transportation Electrification*, 2023.

Author Biography

Tinglong Pan received his B.Eng. degree in Industrial Automation from China University of Mining and Technology, Xuzhou, China, in 1999, and the Ph.D. degree in Power Electronics and Power Drive from China University of Mining and Technology, Xuzhou, China, in 2004.

He is currently a Professor at Jiangnan University, China, where his research interests include microgrid control technology, power conversion technology, power drive system and its intelligent control technology.

Chuanjun Gong received his bachelor's degree in Electrical Engineering and Automation from Tongling University, China, in 2022. He is currently studying for a master's degree in Electrical Engineering at Jiangnan University, China.

His research interests mainly include battery fault diagnosis and deep learning algorithm development.

Dezhi Xu received the Ph.D. degree in Control Theory and Control Engineering from Nanjing University of Aeronautics and Astronautics, China, in 2013.

He was a Visiting Fellow with the Department of Biomedical Engineering, City University of Hong Kong, China, from 2018 to 2019. He is currently a Professor and Doctoral Supervisor with the Southeast University, China. His research interests include data-driven control, fault diagnosis and fault-tolerant control, multi-agent systems and cyber-physical systems, technologies of renewable energy, motor control, and smart grid. Dr. Xu was supported by the National Natural Science Fund for Excellent Young Scientists Fund Program in 2022. He was a recipient of the First Class Prize of Science and Technology Progression from the China General Chamber of Commerce in 2016, and the Best Young Scholar of Jiangnan University in 2022. He was a Guest Editor for the International Journal of Innovative Computing, Information and Control and the Electric Power. He currently serves as an Editorial Board Member for the International Journal of Innovative Computing, Information and Control, the Electric Power, the Electrotechnical Application and the Electrical Engineering. He is a Committee Member of the Association of Energy Internet, and Trusted Control in Chinese Association of Automation (CAA), and the Energy Storage in China Renewable Energy Society (CRES).

Weilin Yang received his B.Eng. degree in Machine Design & Manufacture and Their Automation from University of Science and Technology of China, Hefei, China, in 2009, and the Ph.D. degree in Mechanical Engineering from City University of Hong Kong, Hong Kong SAR, China, in 2013.

He was a postdoctoral researcher at Masdar Institute of Science and Technology (now Khalifa University), Abu Dhabi, UAE, 2013-2016. He was a research engineer of General Electric (GE) Global Research, Shanghai, China, 2016-2017. He joined Jiangnan University, China, in July 2017, where he is currently an Associate Professor. His research interests include modeling and control of energy systems, robust model predictive control, and dada-driven control.

Yujian Ye received the B.Eng. (Hons) degree in Electrical and Electronic Engineering from Northumbria University, Newcastle Upon Tyne, U.K., in 2011, the M.Sc. degree with Distinction in Control Systems and the Ph.D. degree from Imperial College London, London, U.K., in 2013 and 2017, respectively. He performed Postdoctoral research also with Imperial College London, London, U.K., from 2016 to 2020, and then joined Southeast University, Nanjing, China with Associate Professorship in 2021.

He is currently a Professor with Young Endowed Chair Honor with the School of Electrical Engineering at Southeast University, China, and an Honorary Lecturer at Imperial College London, U.K. His current research interests include development and application of novel data analytics and artificial intelligence techniques in low-carbon energy-transportation-information systems modeling, analysis and control, and optimization of economics of power system operation and planning. He serves as the Associate Editor of several prestigious and reputable international journals, including IEEE Transactions on Smart Grid, IEEE Transactions on Industrial Informatics and IEEE Transactions on Industry Applications. He also serves as the Subject Editor of "Emerging Technologies in Smart Grids" for IET Smart Grid, and a Young Editorial Board Member of Applied Energy and cross-disciplinary journal Nexu.